Comparison of Downscaled Precipitation Data over a Mountainous Watershed: A Case Study in the Heihe River Basin

XIAODUO PAN AND XIN LI

Cold and Arid Regions Environmental and Engineering Research Institute, Chinese Academy of Sciences, Lanzhou, China

KUN YANG

Laboratory of Tibetan Environment Changes and Land Surface Processes, Institute of Tibetan Plateau Research, Chinese Academy of Sciences, Beijing, China

JIE HE

Laboratory of Tibetan Environment Changes and Land Surface Processes, Institute of Tibetan Plateau Research, and State Key Laboratory of Numerical Modeling for Atmospheric Sciences and Geophysical Fluid Dynamics, Institute of Atmospheric Physics, Chinese Academy of Sciences, Beijing, China

YANLIN ZHANG AND XUJUN HAN

Cold and Arid Regions Environmental and Engineering Research Institute, Chinese Academy of Sciences, Lanzhou, China

(Manuscript received 28 November 2013, in final form 5 March 2014)

ABSTRACT

Development of an accurate precipitation dataset is of primary importance for regional hydrological process studies and water resources management. Here, four regional precipitation products are evaluated for the Heihe River basin (HRB): 1) a spatially and temporally disaggregated Climate Prediction Center Merged Analysis of Precipitation (CMAP) at 0.25° spatial resolution (DCMAP); 2) a fusion product obtained by merging China Meteorological Administration station data and Tropical Rainfall Measuring Mission precipitation data at 0.1° spatial resolution supported by the Institute of Tibetan Plateau Research (ITP), Chinese Academy of Sciences (ITP-F); 3) a disaggregated CMAP downscaled by a statistical meteorological model tool at 1-km spatial resolution (DCMAP–MicroMet); and 4) a Weather Research and Forecasting (WRF) Model simulation with 5-km resolution (WRF-P). The validation metrics include spatial pattern, temporal pattern, error analysis with respect to observation data, and precipitation event verification indicators. The results indicate that 1) precipitation from the DCMAP product may not be suitable for water cycle studies at the watershed scale because of its coarser spatial resolution and 2) ITP-F, WRF-P, and DCMAP–MicroMet precipitation products generally show similar spatial–temporal patterns in HRB but have varying performances between different subbasins.

1. Introduction

The Fourth Assessment Report of the Intergovernmental Panel on Climate Change (Pachauri and Reisinger 2007) pointed out that the lack of data with high spatial and temporal resolution and long time series is a key source of uncertainties in understanding regional vulnerability to climate change and in developing appropriate countermeasures. Meteorological data with high spatial and temporal resolution are in urgent demand for many purposes. In particular, precipitation is one of the most important variables affecting the exchange of moisture and heat between the atmosphere and the land surface (Fekete et al. 2004; Gottschalck et al. 2005; Tian et al. 2007), and the development of an accurate precipitation dataset is of primary importance for regional hydrological process studies and water resources management (Wilk et al. 2006; Immerzeel et al. 2009; Sorooshian et al. 2011).

Corresponding author address: Xiaoduo Pan, Cold and Arid Regions Environmental and Engineering Research Institute, Chinese Academy of Sciences, Lanzhou 730000, China.
E-mail: panxiaoduo@lzb.ac.cn

DOI: 10.1175/JHM-D-13-0202.1

There are three basic kinds of precipitation estimate (Prigent 2010): ground observations, satellite estimates, and numerical modeling. The ground observations include rain gauges and weather radars; the satellite estimation may use near-infrared (NIR), passive microwave, and active microwave sensors; and the numerical modeling can be based on either global or regional numerical models.

In general, rain gauges are considered to be the source of reference values at a given location and are the basis for evaluating satellite or numerical modeling products. Ground radars measure precipitation at a fine resolution and may also be used to validate satellite precipitation estimates (Amitai et al. 2012). In addition, disdrometers are considered to be an aid to ground observations and are used to distinguish precipitation type and measure the drop size distribution (DSD) at a given location to assess/calibrate the equivalent radar reflectivity factor Z and to build more reasonable equations between Z and rainfall intensity (Z–R relations) for various types of rain. However, radar and disdrometers are not used in the precipitation products discussed in this paper.

The distribution of ground observations is uneven and sparse, whereas satellite estimates can overcome this disadvantage and can provide spatially continuous precipitation data. NIR-based precipitation estimates have high spatial–temporal resolution, but the relationship between the cold cloud tops and surface rainfall is indirect. Representative NIR satellites are the Geostationary Operational Environmental Satellite (GOES), the Geostationary Meteorological Satellite (GMS), FY-3B, Meteosat, and Multifunctional Transport Satellites (MTSAT). Microwave-based precipitation estimates cover the globe and have a more accurate calibration, but their spatial–temporal resolution is coarse. Representative passive microwave products are the Special Sensor Microwave Imager (SSM/I), the Special Sensor Microwave Image/Sounder (SSM/IS), the Advanced Microwave Scanning Radiometer for Earth Observing System (EOS; AMSR-E), and the Advanced Microwave Scanning Radiometer 2 (AMSR2). Representative active microwave products are the Tropical Rainfall Measuring Mission (TRMM; Kummerow et al. 1998) and the Global Precipitation Measurement (GPM; Smith et al. 2007); the GPM mission was launched in 2014.

Numerical modeling can provide spatially and temporally consistent precipitation products. In general, global numerical models and global reanalysis can describe precipitation distribution patterns at a 100-km scale; regional numerical models describe weather at 10–100-km scales and even much finer spatial scales. Regional numerical model simulations are often initiated and bounded by global numerical model output or reanalysis data, so regional numerical model simulations are also called dynamic downscaling. Precipitation has proven to be the most difficult parameter to be simulated in numerical models because of our limited understanding of precipitation phenomena.

In addition to the above basic precipitation products, other approaches have been developed to create accurate precipitation products, such as merging various precipitation estimates, assimilating observation data into a numerical model, and ensemble forecasts.

Many global precipitation datasets have been developed based on these measurements and techniques. The Climatic Research Unit (CRU; New et al. 1999, 2000), the Global Precipitation Climatology Project (GPCP; Adler et al. 2003), the U.S. Climate Prediction Center (CPC; Chen et al. 2002), the German Weather Service Global Precipitation Climatology Centre (GPCC; Beck et al. 2004), the CPC Merged Analysis of Precipitation (CMAP; Xie and Arkin 1996), and TRMM (Huffman et al. 2007) are global precipitation products (more information on global precipitation datasets can be found at www.isac.cnr.it/~ipwg/data/datasets.html).

However, precipitation variability over complex terrain is difficult to estimate, especially at small spatial scales (Johnson and Hanson 1995), where rain gauges are often unevenly and sparsely deployed. Downscaling methods have been developed to apply coarser-resolution precipitation data to a watershed-scale region. Various physically based statistical models have been developed to downscale spatially low-resolution precipitation fields and establish long-term and appropriately scaled precipitation products for mountainous terrain (Daly et al. 1994; Wilby and Wigley 2000; Brown and Comrie 2002; Guan et al. 2009). A number of downscaled precipitation fields obtained by coupling regional numerical models with hydrological models have been applied for flood forecasting, runoff simulation, and decision-support system development (Anderson et al. 2002; Evans 2003; Kotlarski et al. 2005; Lin et al. 2006; Kunstmann et al. 2008). The basis of these applications is acceptable accuracy of precipitation data, so evaluation of the accuracy of downscaled precipitation and of the downscaling methods in a specific region has become necessary (Colle et al. 1999; Su et al. 2008; Zong and Wang 2011; Ward et al. 2011).

The Heihe River basin (HRB) is a relatively large mountainous watershed for precipitation evaluation, owing to its complex terrain and diverse landscapes from upstream to downstream, with glaciers, frozen soil, alpine meadow, forest, irrigated crops, riparian ecosystems, and the Gobi desert. The HRB is a typical inland river basin in an arid region, where there is severe conflict between the water demands of ecosystems

TABLE 1. Data sources used in this study.

Product	Spatial resolution	Temporal resolution	Time period available	Source of data
DCMAP	0.25°	3 hourly	2001–present	Goddard Earth Sciences Data and Information Services Center (Rodell et al. 2004)
ITP-F	0.1°	3 hourly	1998–2010	ITP, Chinese Academy of Sciences (Chen et al. 2011)
WRF-P	5 km	Hourly	1999–present	National Center for Atmospheric Research (Skamarock et al. 2008)
DCMAP–MicroMet	1 km	Hourly	2001–present	MicroMet Group (Liston and Elder 2006)

and economic development (Li et al. 2013). In addition, HRB precipitation has shown considerable spatiotemporal variation, and 10 years of observations at stations supported by the China Meteorological Administration (CMA) have indicated that around 70% of precipitation occurred from June to September, while only 5% occurred from November to the following February; annual precipitation was around 400 mm yr^{-1} in the upstream region of the HRB, around 100 mm yr^{-1} in the central region, and around 50 mm yr^{-1} in the downstream region. The lack of abundant precipitation observations and long-term regional precipitation products has limited many hydrological and ecological simulations in the HRB (Chen et al. 2006; Kang et al. 2008; Yin et al. 2013). Because of this lack of data and the complexity of precipitation patterns over the HRB, a wireless observation network will be installed by the Heihe Watershed Allied Telemetry Experimental Research (HiWATER) project (Li et al. 2013). Five self-recording rain gauges recently supported by the Watershed Allied Telemetry Experimental Research (WATER) project (Li et al. 2009) are included in this paper; these gauges are independent of any analyses, some of which use some of the CMA gauges.

In this paper, four regional downscaled precipitation products are evaluated over the HRB: 1) a spatially and temporally disaggregated CMAP (DCMAP; see Rodell et al. 2004) at 0.25° spatial resolution; 2) a fusion product obtained by merging CMA station data and TRMM precipitation data (TRMM 3B42; see Huffman et al. 2007) at 0.1° spatial resolution supported by the Institute of Tibetan Plateau Research (ITP), Chinese Academy of Sciences (named ITP-F); 3) DCMAP downscaled by a statistical meteorological model (MicroMet; see Liston and Elder 2006) tool at a 1-km spatial resolution (named DCMAP–MicroMet); and 4) a Weather Research and Forecasting (WRF) Model (see Michalakes et al. 1998, 2001) simulation with 5-km resolution (named WRF-P). These four products cover satellite estimates, ground observations, and downscaling methods. The downscaling methods include dynamic downscaling, statistical downscaling, interpolation, and merging methods. The main aims of this paper are 1) to use different spatial-resolution precipitation data to determine the appropriate scale for watershed regions; 2) to evaluate the precipitation patterns in complex mountainous regions; 3) to comprehensively validate the above four precipitation products; and 4) to find a reasonable method based on multiple sources to build long-term precipitation products for complex mountainous regions at the watershed scale. The next section describes these four products in detail, section 3 introduces the validation methods and the research region, section 4 presents the results, and section 5 comprises the discussion and conclusions.

2. Summary of precipitation products over the HRB

Table 1 summarizes the spatial resolution, temporal resolution, time period coverage, and source of data for the four precipitation products.

a. DCMAP

One of the optional precipitation forcings for the Global Land Data Assimilation System (GLDAS; see Rodell et al. 2004) is the CMAP (see Xie and Arkin 1996, 1997) at 2.5°, which is a blend of satellite (IR and microwave) and gauge observations and was then spatially and temporally disaggregated by Global Data Assimilation System (GDAS) modeled precipitation fields to match the GLDAS resolution of 0.25°. This precipitation product (named DCMAP) was accessed at the Hydrology Data and Information Services Center (HDISC) and was adopted as one of the precipitation sources evaluated in the HRB.

b. China Meteorological Forcing Dataset

The China Meteorological Forcing Dataset was developed by merging a variety of data sources at the Institute of Tibetan Plateau Research (ITP), Chinese Academy of Sciences (He 2010). This product is also called the ITP-forcing (ITP-F). It has been used for land surface modeling in China (Chen et al. 2011). The inputs for the precipitation data fusion are CMA measurements at 740 stations and TRMM satellite precipitation analysis data (3B42v6) (Huffman et al. 2007). This

product is provided at a spatial resolution of 0.1° and a temporal resolution of 3 h.

The precipitation product is produced by the following general procedures. First, TRMM 3B42v6 precipitation data are bilinearly interpolated at the 740 CMA stations and aggregated from 3 h to 1 day. Then, the differences between the measurement and the TRMM 3B42v6 values at the stations are interpolated into gridded values at a spatial resolution of 0.1° by the ANUSPLIN package (Hutchinson 1995). The TRMM 3B42v6 precipitation data are then bilinearly resampled into grid values at the same spatial resolution from 0.25°. Last, if the resampled TRMM precipitation grid point value is greater than 0, the precipitation is obtained by adding the gridded TRMM precipitation value and the gridded difference between the TRMM value and the measurement; otherwise, 0 is retained as the final precipitation product. If the TRMM value is less than the interpolated difference, zero is assigned to prevent negative values.

c. WRF-P

The WRF is a modern mesoscale numerical weather prediction system that serves both operational and research communities. The model uses a terrain-following hydrostatic pressure coordinate system with permitted vertical grid stretching (Laprise 1992). Arakawa C grid staggering (Arakawa and Lamb 1977) is used for horizontal discretization. A detailed description of WRF was presented in Skamarock et al. (2008). In the present study, WRF was used for downscaling of weather and climate ranging from 1 km to thousands of kilometers and was then used for deriving meteorological parameters required for hydrological models. The model was initialized by real boundary conditions using the National Centers for Environmental Prediction (NCEP) Final Analysis (FNL) data (NCAR 2014), with a resolution of 1° × 1°. Two-way nested computational domains of 40 × 54 × 27 and 100 × 120 × 27 grid points at horizontal resolutions of 25 km and 5 km, respectively, were used. The first domain covers most of Gansu Province, ranging from 32.6° to 47.4°N in latitude and from 92.4 to 107.6°E in longitude (shown in Fig. 1). The second domain covers the HRB, ranging from 37° to 43°N in latitude and from 96.6° to 103.4°E in longitude. A ratio of 1:5 was maintained between resolutions of the outer domain and FNL data to ensure reliable boundary conditions for the model. The model's physical configuration is summarized in Table 2.

d. DCMAP–MicroMet

The DCMAP precipitation product was interpolated into the spatial–temporal precipitation products with a spatial resolution of 1 km and a temporal resolution of 1 h with the MicroMet tool. MicroMet, of intermediate complexity and quasi-physical basis, has been developed to produce the high-resolution (e.g., 30-m to 1-km horizontal grid increment) atmospheric forcing required to drive spatially distributed terrestrial models over a wide variety of landscapes (Liston and Elder 2006). In the present study, the 3-h interval precipitation data were first converted into 1-h interval precipitation data by a smoothing method in a 7-h time window. Spatial interpolation was carried out after the processing of the time series. The Barnes objective analysis scheme (Barnes 1964) was used to interpolate the DCMAP grid values to high-spatial-resolution gridded data. The variable P (mm h^{-1}) is computed from

$$P = P_0 \left[\frac{1 + \chi(z - z_0)}{1 - \chi(z - z_0)} \right], \tag{1}$$

where P_0 (mm h^{-1}) is the DCMAP forcing-data precipitation at a spatial resolution of 0.25°, z_0 (m) is the grid elevation at a spatial resolution of 0.25°, z (m) is the grid elevation at a spatial resolution of 0.01°, and χ (km^{-1}) is a seasonally varying factor (Thornton et al. 1997). Here, χ is determined using 10-yr time series of precipitation from CMA stations within or around the HRB. Owing to the uneven distribution of these stations, χ strongly influences the interpolation of DCMAP.

3. Research region, validation data, and verification indicators

a. Research region

The HRB is the second largest inland river basin in China (shown in Fig. 1). It is located at 37°45′–42°45′N and 97°–102°E and covers an area of approximately 140 000 km^2. Based on the terrain relief characteristics, the HRB can be divided into three parts: upstream, center, and downstream. The upstream region is the source region of the HRB, and the dominant topography is high mountains and deep gorges. On the cold mountain tops, evaporation is weak, the average annual temperature ranges from −3.1° to 3.6°C, and the average annual precipitation is from 350 to 450 mm (Cao and Dou 2005; Song et al. 2003). The zone of maximum precipitation lies between 4500 and 4700 m (Wang et al. 2009), and on the high mountains the snow distribution is relatively stable. In the central region, the dominant topography is flat terrain, the average annual temperature is 7°–8.2°C (significantly higher than that in the upstream region), and the annual precipitation is 80–120 mm (Cao and Dou 2005; Song et al. 2003). In the downstream region, with the exception of the lake

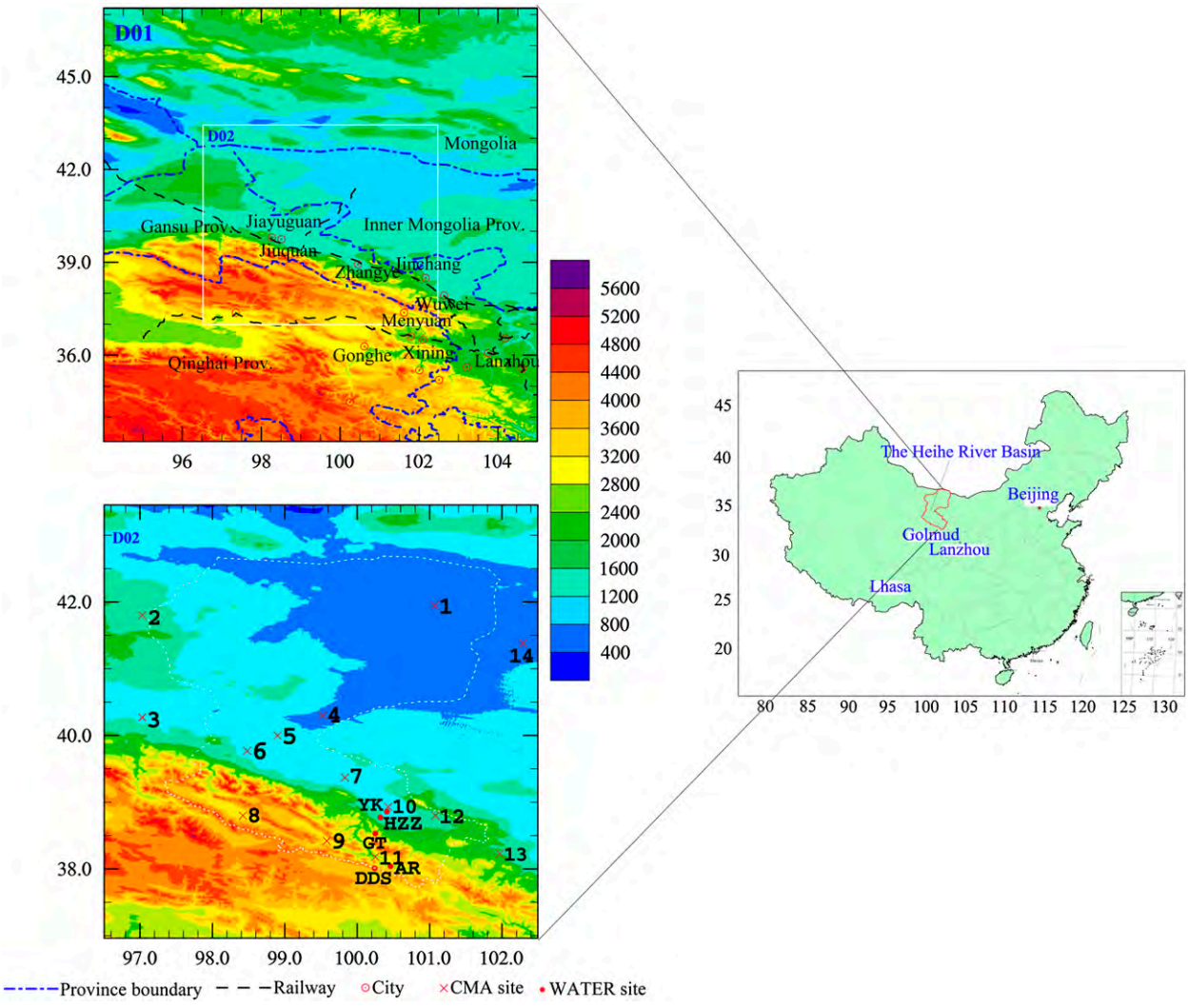

FIG. 1. Nesting domain configuration for the numerical experiment (red crosses denote CMA stations; numbers indicate stations: 1) Ejin, 2) Mazongshan, 3) Yumen, 4) Dingxin, 5) Jinta, 6) Jiuquan, 7) Gaotai, 8) Tuole, 9) Yeniugou, 10) Zhangye, 11) Qilian, 12) Shandan, 13) Yongchang, and 14) Guaizihu.

shorelines of Juyan Lake and Ejin delta, most of the landscape consists of the Gobi desert (much of the Gobi is not sandy but has exposed bare rock), where the annual precipitation is from 40 to 60 mm (Cao and Dou 2005; Song et al. 2003).

b. *Validation data and verification indicators*

There are 14 CMA daily rain gauges distributed throughout the entire HRB and five continuously operating WATER hourly rain gauges in the upstream

TABLE 2. WRF physical configuration in this study.

Physics processes	Domain 1 (25 km)	Domain 2 (5 km)
Horizontal	40 × 54	100 × 120
Time interval	150 s	30 s
Microphysics	Lin et al. (2006) scheme	Lin et al. (2006) scheme
Cumulus parameterization	Kain–Fritsch scheme	Kain–Fritsch scheme
PBL	Yonsei University scheme	Yonsei University scheme
Radiation	Dudhia scheme	Dudhia scheme
Surface–land	Noah LSM	Noah LSM
Initial and Boundary data	NCEP/FNL analysis	Domain 1

TABLE 3. Contingency table comparing observations and the four precipitation products (set yes if daily precipitation ≥0.1 mm h^{-1}; otherwise, set no).

		DCMAP		ITP-F		WRF		DCMAP–MicroMet		
		Yes	No	Yes	No	Yes	No	Yes	No	Sum
Obs	Yes	218	0	172	47	188	30	195	23	218
	No	242	0	63	178	97	145	105	137	242
	Sum	460	0	235	225	285	175	300	160	460

region of HRB. The geographical features of these stations' positions are shown in Fig. 1.

Analysis of spatial and seasonal patterns of precipitation, error analysis based on comparison with rain gauge data, and evaluations of precipitation events are presented below. The total precipitation and spatial patterns of the upstream, central, and downstream regions of the HRB for 2008 were analyzed separately. The mean bias error (MBE) of precipitation was calculated at the CMA stations for all of 2008 and at the WATER stations: Arou (AR), Dadongshu (DDS), and Huazhaizi (HZZ) from June to August 2008 and Guantan (GT) and Yingke (YK) from June to August 2010. The indictors, which include probability of detection (POD), threat score (TS), false alarm ratio (FAR), frequency bias (FBI) and equitable threat score (ETS), were used to evaluate the daily precipitation events from June to August at the five WATER stations. POD can be regarded as the fraction of occasions when an event occurred that was also forecast. TS can be viewed as the proportion of correct forecasts of the quantity being forecast after removal of correct "no" forecasts. FAR is the fraction of "yes" forecasts that turn out to be wrong, equivalent to the proportion of forecast events that fail to materialize. The FBI has a range of possible values from 0 to ∞, but its ideal value is 1, indicating an unbiased forecast where the event is forecast exactly as often as it is observed. ETS is the ratio of the correct forecast area to the total area of the forecast and observed precipitation, which can vary from a small negative number to 1.0, where 1.0 represents a perfect forecast.

The POD, TS, FAR, FBI, and ETS indicators were derived using a contingency table approach (Wilks 1995) and were used to evaluate precipitation events in the HRB from June to August. Higher POD, TS, and ETS values, lower FAR values, and smaller deviations of FAR from unity all indicate better estimates. Five stations were selected, the number of station days was 92, and the actual number of rainy days for these five stations was 218. Table 3 is the daily precipitation event contingency table comparing observations and the four precipitation products. Based on the contingency table, values of POD, TS, FAR, FBI, and ETS were calculated from Eqs. (2) to (6) below. Fifteen thresholds were set, from 0.1 to 15 mm day^{-1}.

The equations are as follows:

$$\mathrm{POD} = \frac{N_{11}}{N_{11} + N_{10}}, \tag{2}$$

$$\mathrm{TS} = \frac{N_{11}}{N_{11} + N_{10} + N_{01}}, \tag{3}$$

$$\mathrm{FAR} = \frac{N_{01}}{N_{01} + N_{11}}, \tag{4}$$

$$\mathrm{FBI} = \frac{N_{11} + N_{01}}{N_{10} + N_{11}}, \quad \text{and} \tag{5}$$

$$\mathrm{ETS} = \frac{N_{11} - a_{\mathrm{ref}}}{N_{11} - a_{\mathrm{ref}} + N_{10} + N_{01}}$$
$$a_{\mathrm{ref}} = \frac{N_{11} \times N_{00} - N_{10} \times N_{01}}{N_{11} \times N_{00} + N_{10} \times N_{01}}, \tag{6}$$

where N_{11} means the observation is yes (i.e., wet) and the precipitation product estimate is yes, N_{10} means the observation is yes and the precipitation product estimate is no, N_{01} means the observation is no and the precipitation product estimate is yes, and N_{00} means the observation is no and the precipitation product estimate is no.

4. Results

a. Spatial pattern

Figures 2a–d are the spatial patterns of precipitation in the HRB during 2008 from DCMAP, ITP-F, WRF-P, and DCMAP–MicroMet, respectively. Overall, these four products shared some common characteristics: precipitation decreased gradually from south to north, the upstream region had the most precipitation (around 350 mm), the downstream region had the least precipitation (around 50 mm), and the central region was in between. Table 4 lists the annual precipitation flux and precipitation volume in the whole basin and in the upstream, central, and downstream regions in 2008. The coarser DCMAP underestimated precipitation flux in

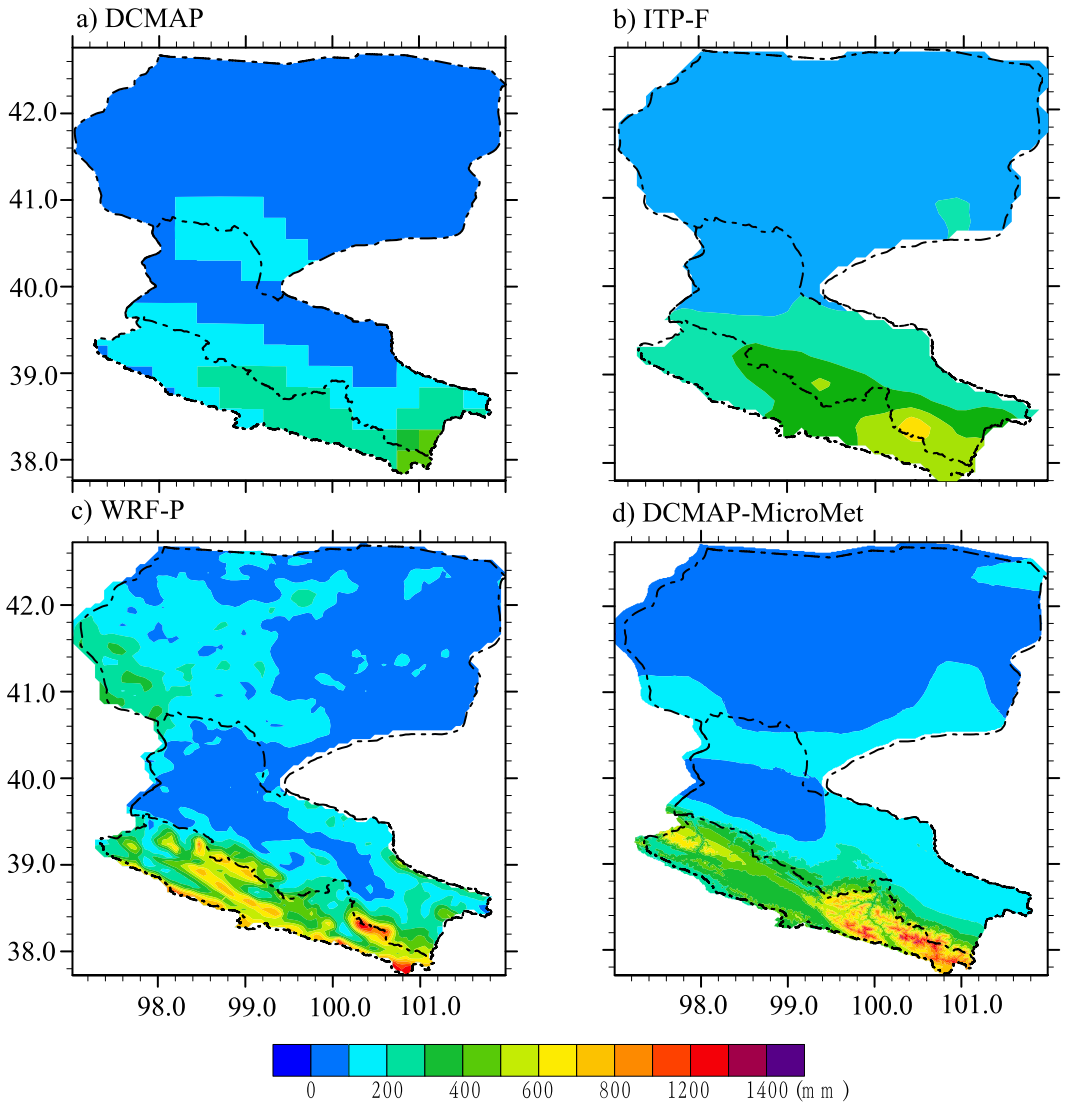

FIG. 2. Comparison of spatial patterns of the four precipitation products in the HRB during 2008.

the upstream region, possible because the upstream region of the HRB has much larger precipitation flux than the other regions; however, the landscape of the upper basin has a much higher fractal index, and in many coarse grids the higher precipitation flux values are excluded from the average in statistical analysis. This caused the annual precipitation for the HRB to be lower than that of the other products.

Precipitation in the HRB occurs mainly in the upstream region. From Figs. 2a–d, we also can see the

TABLE 4. Annual precipitation estimates of four precipitation products for HRB in 2008 (areas are 12.87×10^4, 2.76×10^4, 3.24×10^4, and 6.87×10^4 m^2 for whole, upper, middle, and lower basins, respectively).

		Total precipitation flux (mm yr^{-1})				Total precipitation (10^8 m^3)			
Product	Resolution	Whole	Upper	Middle	Lower	Whole	Upper	Middle	Lower
DCMAP	0.25°	114.3	247.1	129.8	54.0	147.2	68.1	42.0	37.1
ITP-F	0.1°	177.7	360.6	182.0	99.8	228.7	101.1	59.0	68.6
WRF-P	5 km	166.1	406.8	122.0	90.5	213.7	111.9	39.6	62.2
DCMAP–MicroMet	1 km	159.9	428.2	124.1	72.9	205.7	115.4	40.2	50.1

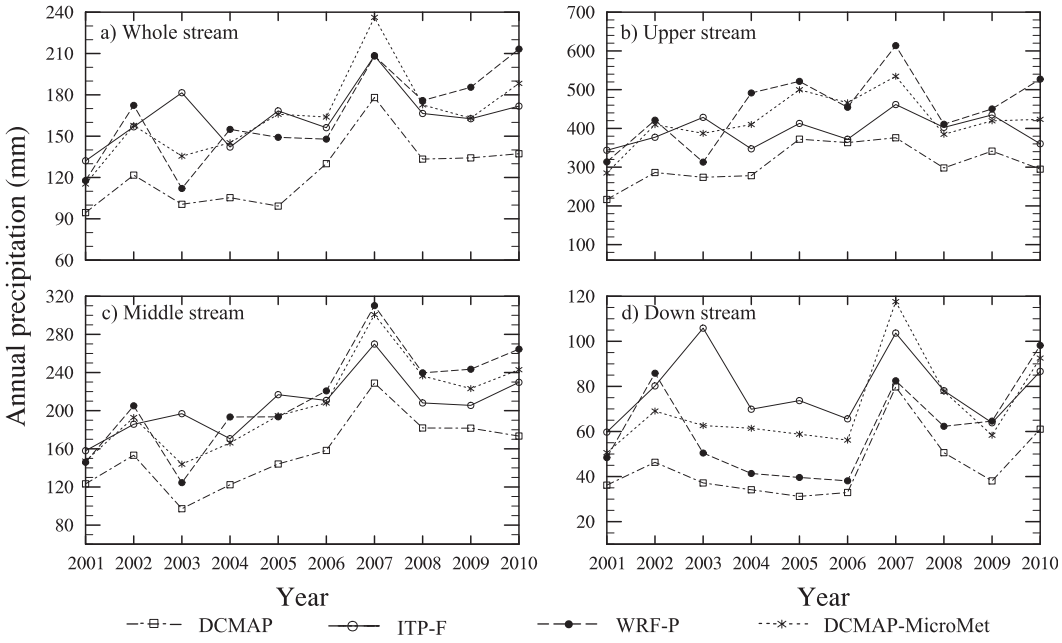

FIG. 3. Annual precipitation fluxes estimated by four precipitation products from 2001 to 2010.

spatial patterns of precipitation in the upstream reach of the HRB in 2008 from DCMAP, ITP-F, WRF-P, and DCMAP–MicroMet, respectively. Overall, these four products shared one common characteristic: precipitation decreased gradually from east to west. Because of the coarse spatial resolution, as mentioned above, the precipitation flux from DCMAP could not describe the watershed scale in detail. The other estimates were somewhat similar to each other, but the spatial patterns were different. The DCMAP–MicroMet precipitation product placed the precipitation maximum in the middle of the eastern end of the basin, ITP-F placed it in the northern part of the eastern end, and WRF-P placed it in the central and southern parts of the eastern end.

b. *Temporal and seasonal patterns*

All precipitation products showed that the precipitation fluxes gradually increased from 2001 to 2010 (Fig. 3), and these four precipitation products had peak fluxes in 2007; all these features are similar to the observations (Fig. 4). Although the DCMAP precipitation fluxes were a little lower than those of the others, the trend of DCMAP precipitation fluxes from 2001 to 2010 was the same as that of the others and similar to the observations in the upstream and central regions (Fig. 4).

The precipitation fluxes in 2003 from WRF-P, DCMAP, and DCMAP–MicroMet had inflection points and were lower than that from ITP-F, possibly because the two international exchange stations (Fig. 4d) were assimilated into the GCM, which provides the boundary data for WRF, and were merged into CPC (which provides the original data for DCMAP precipitation), although the stations in the upstream and parts of

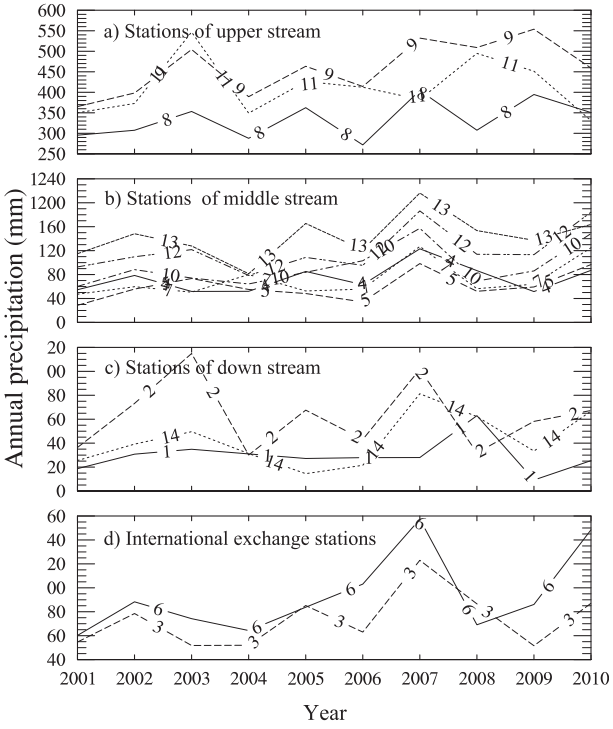

FIG. 4. Annual precipitation fluxes at CMA stations from 2001 to 2010; numbers indicate stations, see Fig. 1.

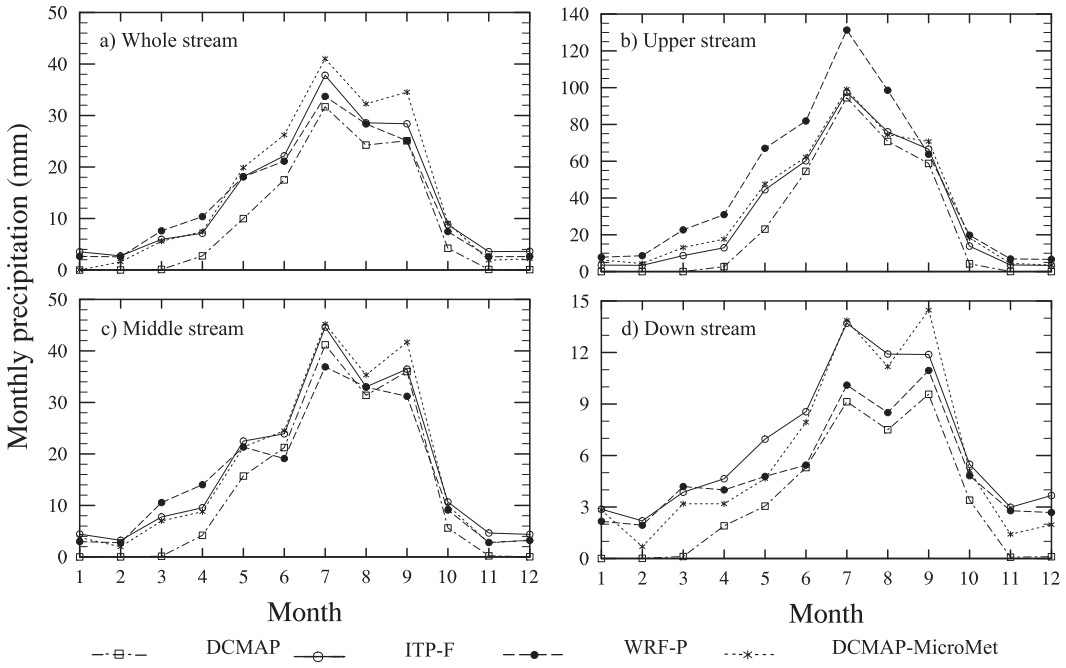

FIG. 5. Monthly precipitation fluxes estimated by four precipitation products for 10 years from 2001 to 2010.

the central region showed no such inflection points in 2003.

Figure 5 shows the average monthly precipitation flux from 2001 to 2010 and indicates that in both the HRB as a whole and in its subbasins, the precipitation mainly occurred in June, July, August, and September. The precipitation in these four months accounted for about three-quarters of the annual total. This characteristic of the precipitation flux in the HRB is consistent with findings in several previous studies (Ding et al. 1999; Song et al. 2003; Cao and Dou 2005; Wang et al. 2009).

c. *Error analysis of the four precipitation products compared with CMA observations for 2008*

Table 5 lists the precipitation flux errors of the four products when compared against 14 CMA observations in 2008. In the upstream region, precipitation flux errors in DCMAP were larger than those of the other products: the greatest deviation was $-273.0\,\mathrm{mm\,yr^{-1}}$, and the

TABLE 5. Errors in the four precipitation products when compared with CMA observations for 2008. The values in bold are the least mean bias error.

Station		Precipitation flux ($\mathrm{mm\,yr^{-1}}$)					Error ($\mathrm{mm\,yr^{-1}}$)			
		Obs	DCMAP	ITP-F	WRF-P	DCMAP- MicroMet	DCMAP	ITP-F	WRF-P	DCMAP- MicroMet
Upper	Tuole	307.6	184.2	255.9	311.5	344.7	−123.4	−51.7	**3.6**	37.1
	Yeniugou	509.1	236.0	411.4	356.5	639.4	−273.1	**−97.7**	−152.6	130.3
	Qilian	484.9	246.1	518.2	192.6	586.0	−238.8	**23.3**	−302.4	101.1
Middle	Yumen	86.6	36.9	135.9	51.1	84.5	−49.7	49.3	−35.5	**−2.1**
	Jinta	56.4	49.7	119.4	58.4	86.9	−6.7	63	**2.0**	30.5
	Jiuquan	36.8	61.8	126.2	42.6	61.8	25.0	89.4	**5.8**	25
	Gaotai	113.9	61.6	186.8	108.7	148.3	−52.3	72.9	**−5.2**	34.4
	Dingxin	52.1	115.2	137.9	73.5	137.9	63.1	85.78	**21.4**	85.8
	Zhangye	153.5	88.4	248.1	84.0	180.5	−65.1	94.6	−69.5	**27.0**
	Shandan	223.7	173.9	299.3	279.8	133.2	**−49.8**	75.6	56.1	−90.5
	Yongchang	194.7	277.9	247.5	212.5	249.2	83.2	52.8	**17.8**	54.5
Lower	Ejin	63.0	51.8	91.3	57.2	55.0	−11.2	28.3	**−5.8**	−8.0
	Mazongshan	32.0	72.8	61.7	53.5	78.9	40.8	29.7	**21.5**	46.9
	Guaizihu	62.2	39.0	77.3	60.4	51.7	−23.2	15.1	**−1.8**	−10.5

lowest was $-125.4\,\mathrm{mm\,yr^{-1}}$. Errors in ITP-F were the smallest: at Qilian station, the error was $23.3\,\mathrm{mm\,yr^{-1}}$, and the errors were -97.7 and $-51.7\,\mathrm{mm\,yr^{-1}}$ at Yeniugou and Tuole, respectively. Errors in WRF-P fluctuated: the error was $3.6\,\mathrm{mm\,yr^{-1}}$ at Tuole station but reached 302.4 and $-152.6\,\mathrm{mm\,yr^{-1}}$ at Yeniugou and Qilian, respectively. In the central basin, errors in WRF-P were smaller than those in the other precipitation products except at Zhangye station and Yumen station. Errors in ITP-F were the largest, and the precipitation flux estimates in ITP-F were far larger than the others, which is why the precipitation flux estimated by ITP-F in the central basin was almost one-third higher than the others. In the lower basin, errors in WRF-P were smaller than those in the other precipitation products. Overall, the precipitation flux simulated by the WRF agreed well with observation data in the central and downstream basins of the HRB. The precipitation flux interpolated from TRMM by ANUSPLIN yielded better results in the upstream region, where terrain is complex.

d. *Event evaluation: A comparison of four precipitation products with WATER data from June to August 2008*

In addition to precipitation flux error analysis, the evaluation of precipitation events is also important for a variable with such high spatial and temporal variability. In the HRB, the precipitation is strongly focused both spatially and temporally: the spatial center is the upstream region, and the temporal center is from June to September. To carry out the analysis for summer, WATER rain gauge data were selected to evaluate the precipitation events from June to August 2008, shown in Fig. 6 (the precipitation from some WATER stations was solid in September, so this month was excluded from the precipitation event analysis). Table 6 lists the precipitation flux errors of the four precipitation products. The precipitation flux errors from WRF-P were 15.6, 10.8, -30.7, and $30.6\,\mathrm{mm\,yr^{-1}}$ at the AR, GT, HZZ, and YK stations, respectively. However, the error reached $181.0\,\mathrm{mm\,yr^{-1}}$ at DDS station in WRF-P. The errors in ITP-F and DCMAP–MicroMet were also high at DDS station. DDS station is located on the south slope of Qilian Shan, which has an altitude of 4146.8 m. Wang et al. (2009) measured a precipitation flux from June to August at Ebao of $360\,\mathrm{mm\,yr^{-1}}$ in 2006. Ebao is located on the north slope of Qilian Shan, and its altitude is around 3500 m. From the elevation lapse rate and a general knowledge of precipitation on Qilian Shan, Chen et al. (2008) determined that the total precipitation on the south slope was greater than that on the northern slope at the same elevation by about 44% in summer 2006. The precipitation flux from June to August at DDS station was deduced to be $500\,\mathrm{mm\,yr^{-1}}$, and the fluxes estimated from ITP-F, WRF-P, and DCMAP–MicroMet were also around $500\,\mathrm{mm\,yr^{-1}}$, so it is reasonable to believe that the observation data may be incorrectly recorded.

At rainfall intensities of 0.1–4 $\mathrm{mm\,day^{-1}}$, Fig. 7 shows that the values of the five indicators remained almost the same for the ITP-F, WRF-P, and DCMAP–MicroMet precipitation products. However, from 6 to 15 $\mathrm{mm\,day^{-1}}$, the values of POD decreased sharply from 0.6 to 0.3, the values of TS decreased from 0.5 to 0.1, the values of FAR increased from 0.4 to 0.8 in the ITP-F and DCMAP–MicroMet precipitation products, and the values of FAR remained lower for the WRF-P precipitation product. The FBI values decreased from 1.0 to 0.6 in ITP-F and DCMAP–MicroMet and increased from 1.4 to 2.1 in WRF-P. In other words, WRF-P inflates the high-end events for precipitation simulation.

5. Discussion and conclusions

In this study, four precipitation products, specifically, DCMAP, ITP-F, WRF-P, and DCMAP–MicroMet, covering ground observations, satellite estimates, numerical models, and ensemble methods, were evaluated in a complex watershed by analysis of their spatial and temporal distribution patterns, in situ error analysis, and verification indicators. Spatial pattern maps were constructed for the whole basin and the upper basin. The interannual and monthly precipitation fluxes for 10 years (2001–10) were calculated to reveal the temporal patterns. Data from 19 rain gauge stations were used for in situ error analysis. Five sets of verification scores were derived based on the number of occurrences in which precipitation products matched the observations.

The results indicate that precipitation from the DCMAP product may not be suitable for water cycle studies at the watershed scale because of its coarser spatial resolution. For example, HRB precipitation is concentrated in the upper basin, where terrain is complex and rainfall processes are diverse, so the DCMAP precipitation product, with a resolution of 0.25°, cannot satisfy the needs of HRB research.

Precipitation dynamically downscaled by the WRF agreed well with CMA observations in the central basin of the HRB but not better than remote sensing products calibrated by CMA observations (ITP-F) in the upper basin. It would be worth trying to assimilate rain gauge data in regional climate models to improve the accuracy of precipitation simulation and forecasting. As far as precipitation event evaluation is concerned, ITP-F, WRF-P, and DCMAP–MicroMet showed equally good performances.

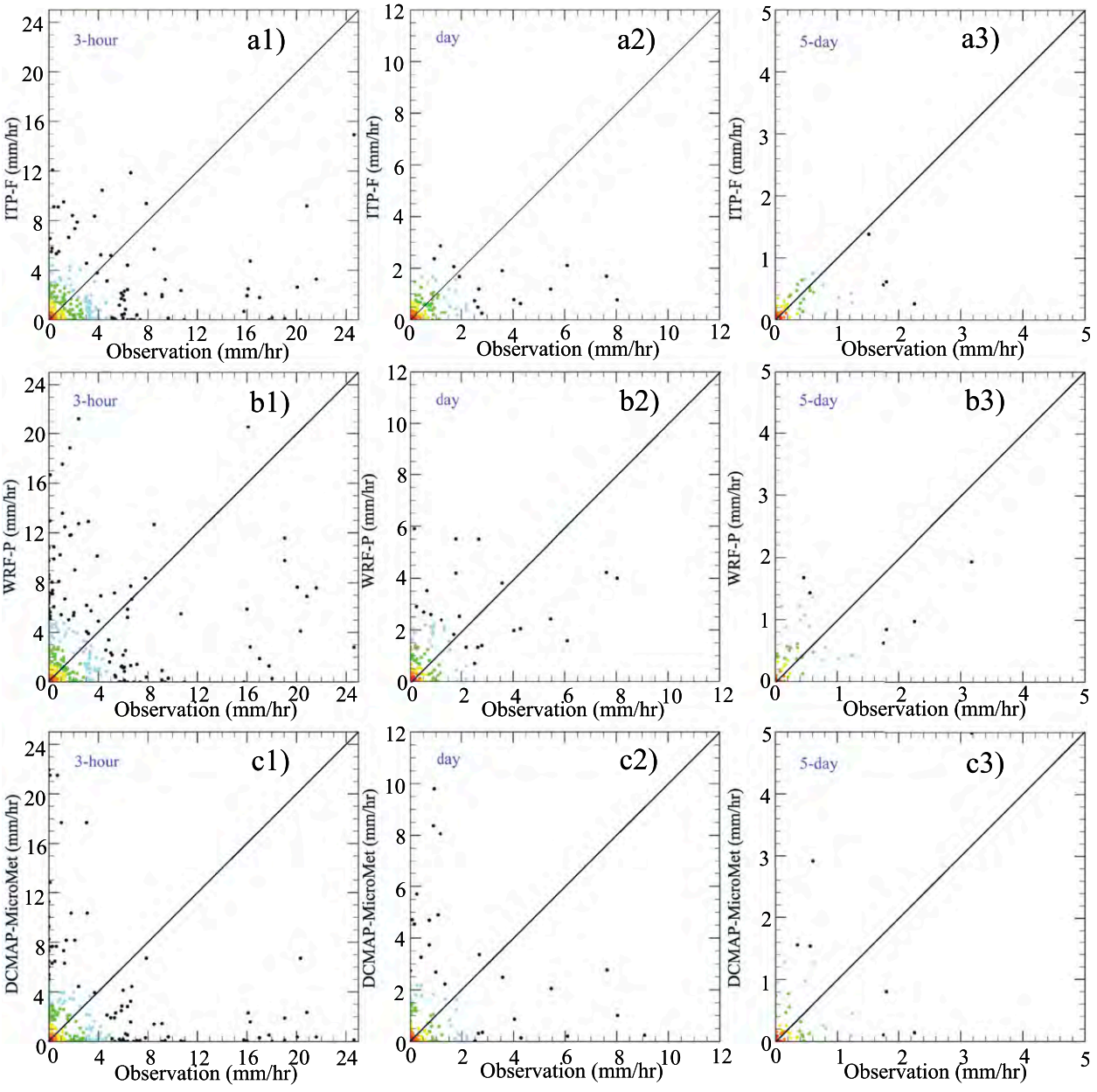

FIG. 6. Two-dimensional scatterplots comparing rainfall events in WATER observations [(a1),(a2),(a3) are for ITP-F at 3-h, daily, and 5-day time scales; (b1),(b2),(b3) are for WRF-P; and (c1),(c2),(c3) are for DCMAP–MicroMet].

The precipitation product estimated by TRMM and interpolated by the ANUSPLIN method, precipitation dynamically downscaled from the NCEP FNL global gridded analysis, and the precipitation product statistically downscaled from DCMAP precipitation data by the MicroMet method can be used as forcing data for ecological and hydrological models and can be important sources of data for water cycle studies after they are corrected by rain gauge data.

In summary, the results from this study indicate that while remote sensing precipitation products such as DCMAP and TRMM can provide global and long-term precipitation estimates in data-scarce areas, currently there are limitations in their accuracy and spatial resolution for watershed-scale studies. The downscaling method is a bridge between the global scale and the regional scale. The DCMAP–MicroMet product statistically downscaled directly from the DCMAP precipitation product by the MicroMet tool, with a spatial resolution of 0.25°, is strongly dependent on the accuracy of DCMAP. It is a potential method for calibrating and interpolating remote sensing precipitation products

TABLE 6. Errors in the four precipitation products when compared with WATER observation data for 2008 from June to August (rain gauge observations and precipitation products for GT and YK are for 2010). The values in bold are the least bias error.

Station		Precipitation flux (mm yr^{-1})					Error (mm yr^{-1})			
		Observation	DCMAP	ITP-F	WRF-P	DCMAP–MicroMet	DCMAP	ITP-F	WRF-P	DCMAP–MicroMet
WATER	AR	250.0	220.8	274.2	265.6	304.5	−29.2	24.2	**15.6**	54.5
	DDS	326.7	220.8	468.9	507.7	512.3	**−105.9**	142.2	181.0	185.6
	GT	139.5	157.0	136.6	150.3	212.0	17.5	**−2.9**	10.8	72.5
	HZZ	80.5	79.6	116.3	49.8	106.1	**−0.9**	35.8	−30.7	25.6
	YK	18.7	79.6	61.1	49.3	56.7	60.9	42.4	**30.6**	38.0

by rain gauge data, such as the ITP-F precipitation product, but it must be noted that the interpolation method (ANUSPLIN) is itself uncertain and is highly dependent on the density of the rain gauge network. Dynamic downscaling based on physical constraints can be used whenever models require small-scale data, but it has many uncertainties in terms of its initial and boundary conditions and its physical parameterizations, especially for complex terrain. Downscaling methods applied without consideration of local factors could fail to generate reliable climate data for areas where the topography is complicated (Custer et al. 1996; Almeida and Landsberg 2003). Regional numerical models are aimed at improving the representation of microphysical processes involved in cloud rain and are also useful in assimilating multiscale precipitation products to improve the initial conditions for generating more accurate precipitation simulation and forecasting. Therefore, although there are current limitations in our comprehensive understanding of the precipitation process, it may be useful to assimilate remote sensing and rain gauge data into regional climate models to yield high-resolution and precise precipitation products.

In addition to the establishment of appropriate-scale precipitation products, use of the rain gauge for evaluation is also open to question. Ground validation sites are a key data source for precipitation evaluation (Asadullah et al. 2008), but there are two issues: 1) systematic errors of rain gauge measurement and 2) representativeness errors between point and areal measurements. Precipitation measurements are affected by systematic errors that lead to an underestimation of actual precipitation. Systematic losses vary by type of precipitation (rain, mixed, snow) and gauge type. For most precipitation gauges, the error depends strongly on the site surroundings, the prevailing wind speeds and the specific gauge form, and more research needs to be conducted on this subject (Sevruk et al. 2009). The representativeness error is defined (Kitchen and Blackall 1992) as the combination of two sources of errors: the spatial representativeness error associated with comparison between a point and an areal average, and the temporal representativeness error associated with the comparison between an accumulation and an integration of a set of instantaneous measurements. These errors must be acknowledged when single rain gauges are used to estimate local-scale spatial means at the daily scale (Bitew and Gebremichael 2010). However, because of limitations to the density of rain gauge networks, it is difficult to convincingly estimate errors in precipitation products across the upstream region of the HRB, especially at the AR and DDS sites. A high-density wireless measurement system is planned for deployment in the near future in the upstream region of the HRB.

The other limitation of this paper is solid precipitation. The accuracy of snow/rainfall also affects the

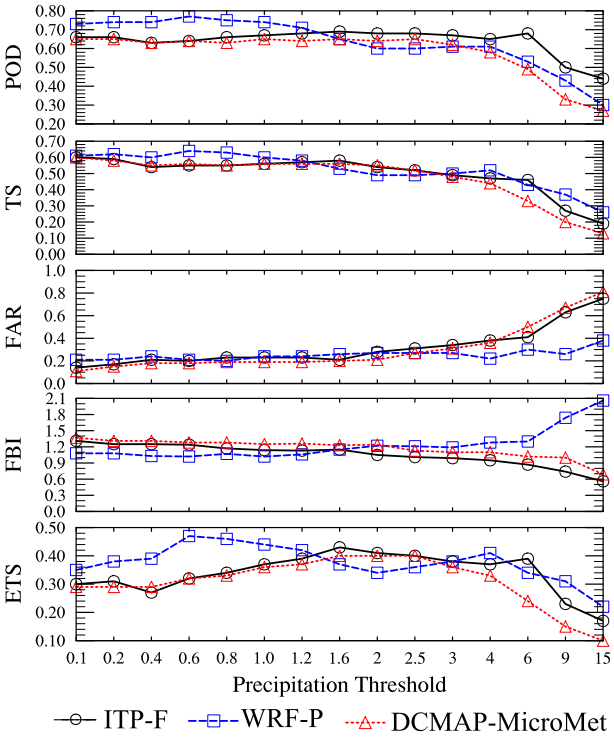

FIG. 7. Verification metrics trend curves across the rainfall thresholds arranged from 0.1 to 15 mm day^{-1}.

results of hydrological model forecasting (Tobin et al. 2012). However, solid precipitation is not distinguished from liquid precipitation at this time, because the liquid and solid precipitation are mixed in some products in our study, so we try to distinguish them by a two-temperature threshold (Han et al. 2010), which uses a gradual change of the proportion of rain and snow based on a linear transition over 2°. However, the weather in the HRB is too complex to use one single criterion, so this issue remains open for future research.

Acknowledgments. This work was supported by the CAS Action Plan for West Development Program (Grant KZCX2-XB3-15) and by grants from the National Natural Science Foundation of China (91125016, 91025004, and 40925004). TRMM 3B42 precipitation data were acquired as part of the mission of NASA's Earth Science Division and were archived and distributed by the Goddard Earth Sciences (GES) Data and Information Services Center (DISC). DCMAP was accessed at the Hydrology Data and Information Services Center (HDISC). The input data for the WRF are from the Research Data Archive (RDA), which is maintained by the Computational and Information Systems Laboratory (CISL) at the National Center for Atmospheric Research (NCAR). The original data are available from the RDA (http://rda.ucar.edu) in dataset number ds083.2. CMA station data were downloaded from the China Meteorological Data Sharing Service System (http://cdc.cma.gov.cn).The NCAR Command Language (NCL; version 6.1.2) is available from UCAR/NCAR/CISL/VETS (http://dx.doi.org/10.5065/D6WD3XH5), Boulder, Colorado. NCL was used for data analysis and graphs in this paper. We acknowledge computing resources and time on the Supercomputing Center of the Cold and Arid Region Environment and Engineering Research Institute of the Chinese Academy of Sciences. The authors thank two anonymous reviewers and the editor for their very helpful comments.

REFERENCES

Adler, R. F., and Coauthors, 2003: The Version 2 Global Precipitation Climatology Project (GPCP) Monthly Precipitation Analysis (1979–Present). *J. Hydrometeor.,* **4,** 1147–1167, doi:10.1175/1525-7541(2003)004<1147:TVGPCP>2.0.CO;2.

Almeida, A. C., and J. J. Landsberg, 2003: Evaluating methods of estimating global radiation and vapor pressure deficit using a dense network of automatic weather stations in coastal Brazil. *Agric. For. Meteor.,* **118,** 237–250, doi:10.1016/S0168-1923(03)00122-9.

Amitai, E., W. Petersen, X. Llort, and S. Vasiloff, 2012: Multiplatform comparisons of rain intensity for extreme precipitation events. *IEEE Trans. Geosci. Remote Sens.,* **50,** 675–686, doi:10.1109/TGRS.2011.2162737.

Anderson, M. L., Z. Q. Chen, M. L. Kavvas, and A. Feldman, 2002: Coupling HEC-HMS with atmospheric models for prediction of watershed runoff. *J. Hydrol. Eng.,* **7,** 312–318, doi:10.1061/(ASCE)1084-0699(2002)7:4(312).

Arakawa, A., and V. R. Lamb, 1977: Computational design of the basic dynamic processes of the UCLA general circulation model. *Methods in Computational Physics,* J. Chang, Ed., Vol. 17, Academic Press, 173–265.

Asadullah, A., N. McIntyre, and M. Kigobe, 2008: Evaluation of five satellite products for estimation of rainfall over Uganda. *J. Hydrol. Sci.,* **53,** 1137–1150, doi:10.1623/hysj.53.6.1137.

Barnes, S. L., 1964: A technique for maximizing details in numerical weather map analysis. *J. Appl. Meteor.,* **3,** 396–409, doi:10.1175/1520-0450(1964)003<0396:ATFMDI>2.0.CO;2.

Beck, C., J. Grieser, and B. Rudolf, 2004: A new monthly precipitation climatology for the global land areas for the period 1951 to 2000. Climate Status Report 2004, German Weather Service Climate Status Rep., 181–190. [Available online at ftp://ftp-anon.dwd.de/pub/data/gpcc/PDF/pdf_28_precipitation.pdf.]

Bitew, M. M., and M. Gebremichael, 2010: Spatial variability of daily summer rainfall at a local-scale in a mountainous terrain and humid tropical region. *Atmos. Res.,* **98,** 347–352, doi:10.1016/j.atmosres.2010.07.008.

Brown, D. P., and A. C. Comrie, 2002: Spatial modeling of winter temperature and precipitation in Arizona and New Mexico, USA. *Climate Res.,* **22,** 115–128, doi:10.3354/cr022115.

Cao, L., and Y. Dou, 2005: The spatial and temporal characteristics and forecasting method of precipitation in Heihe Filed. *Arid Meteor.,* **23,** 35–38.

Chen, M., P. Xie, J. E. Janowiak, and P. A. Arkin, 2002: Global land precipitation: A 50-yr monthly analysis based on gauge observations. *J. Hydrometeor.,* **3,** 249–266, doi:10.1175/1525-7541(2002)003<0249:GLPAYM>2.0.CO;2.

Chen, Q., J. Zhang, and T. Chen, 2008: Synoptic analysis of precipitation process in summer of 2006 over Qilian Mountains. *Arid Meteor.,* **26,** 22–28.

Chen, R. S., E. S. Kang, J. P. Yang, J. S. Zhang, and S. G. Wang, 2006: Application of Topmodel to simulate runoff from Heihe mainstream mountainous basin. *J. Desert Res.,* **23,** 428–434.

Chen, Y. Y., K. Yang, J. He, J. Qin, J. C. Shi, J. Y. Du, and Q. He, 2011: Improving land surface temperature modeling for dry land of China. *J. Geophys. Res.,* **116,** D20104, doi:10.1029/2011JD015921.

Colle, B. A., K. J. Westrick, and C. F. Mass, 1999: Evaluation of MM5 and Eta-10 precipitation forecasts over the Pacific Northwest during the cold season. *Wea. Forecasting,* **14,** 137–156, doi:10.1175/1520-0434(1999)014<0137:EOMAEP>2.0.CO;2.

Custer, S. G., P. Farnes, J. P. Wilson, and R. D. Snyder, 1996: A comparison of hand- and spline-drawn precipitation maps for mountainous Montana. *J. Amer. Water Resour. Assoc.,* **32,** 393–405, doi:10.1111/j.1752-1688.1996.tb03461.x.

Daly, C., R. P. Neilson, and D. L. Phillips, 1994: A statistical topographic model for mapping climatological precipitation over mountainous terrain. *J. Appl. Meteor.,* **33,** 140–158, doi:10.1175/1520-0450(1994)033<0140:ASTMFM>2.0.CO;2.

Ding, Y. J., B. S. Ye, and W. J. Zhou, 1999: Temporal and spatial precipitation distribution in the Heihe catchment, northwest China, during the past 40 a. *J. Glaciol. Geocryology,* **21,** 42–48.

Evans, J. P., 2003: Improving the characteristics of streamflow modeled by regional climate models. *J. Hydrol.,* **284,** 211–227, doi:10.1016/j.jhydrol.2003.08.003.

Fekete, B. M., C. J. Vorosmarty, J. O. Roads, and C. J. Willmott, 2004: Uncertainties in precipitation and their impact on runoff estimates. *J. Climate,* **17,** 294–304, doi:10.1175/1520-0442(2004)017<0294:UIPATI>2.0.CO;2.

Gottschalck, J., J. Meng, M. Rodell, and P. Houser, 2005: Analysis of multiple precipitation products and preliminary assessment of their impact on Global Land Data Assimilation System land surface states. *J. Hydrometeor.,* **6,** 573–598, doi:10.1175/JHM437.1.

Guan, H., J. L. Wilson, and H. Xie, 2009: A cluster-optimizing regression-based approach for precipitation spatial downscaling in mountainous terrain. *J. Hydrol.,* **375,** 578–588, doi:10.1016/j.jhydrol.2009.07.007.

Han, C., R. Shen, J. Liu, Y. Yang, and W. Qing, 2010: A discuss of the separating solid and liquid precipitations. *J. Glaciol. Geocryology,* **32,** 249–256.

He, J., 2010: Development of surface meteorological dataset of China with high temporal and spatial resolution. M.S. thesis, Institute of Tibetan Plateau Research, Chinese Academy of Sciences, 96 pp.

Huffman, G. J., and Coauthors, 2007: The TRMM Multisatellite Precipitation Analysis (TMPA): Quasi-global, multiyear, combined-sensor precipitation estimates at fine scales. *J. Hydrometeor.,* **8,** 38–55, doi:10.1175/JHM560.1.

Hutchinson, M. F., 1995: Interpolating mean rainfall using thin plate smoothing splines. *Int. J. Geogr. Inf.,* **9,** 385–403, doi:10.1080/02693799508902045.

Immerzeel, W. W., M. M. Rutten, and P. Droogers, 2009: Spatial downscaling of TRMM precipitation using vegetation response on the Iberian Peninsula. *Remote Sens. Environ.,* **113,** 362–370, doi:10.1016/j.rse.2008.10.004.

Johnson, G. L., and C. Hanson, 1995: Topographic and atmospheric influences on precipitation variability over a mountainous watershed. *J. Appl. Meteor.,* **34,** 68–87, doi:10.1175/1520-0450-34.1.68.

Kang, E. S., R. S. Chen, Z. H. Zhang, X. B. Ji, and B. W. Jin, 2008: Some problems facing hydrological and ecological researches in the mountain watershed at the upper stream of an inland river basin. *Adv. Earth Sci.,* **23,** 675–681.

Kitchen, M., and R. M. Blackall, 1992: Representativeness errors in comparisons between radar and gauge measurements of rainfall. *J. Hydrol.,* **134,** 13–33, doi:10.1016/0022-1694(92)90026-R.

Kotlarski, S., A. Block, U. Böhm, D. Jacob, K. Keuler, R. Knoche, D. Rechid, and A. Walter, 2005: Regional climate model simulations as input for hydrological applications: Evaluation of uncertainties. *Adv. Geosci.,* **5,** 119–125, doi:10.5194/adgeo-5-119-2005.

Kummerow, C., W. Barnes, T. Kozu, J. Shiue, and J. Simpson, 1998: The Tropical Rainfall Measuring Mission (TRMM) sensor package. *J. Atmos. Oceanic Technol.,* **15,** 809–816, doi:10.1175/1520-0426(1998)015<0809:TTRMMT>2.0.CO;2.

Kunstmann, H., G. Jung, S. Wagner, and H. Clottey, 2008: Integration of atmospheric sciences and hydrology for the development of decision support systems in sustainable water management. *Phys. Chem. Earth,* **33,** 165–174, doi:10.1016/j.pce.2007.04.010.

Laprise, R., 1992: The Euler equation of motion with hydrostatic pressure as independent coordinate. *Mon. Wea. Rev.,* **120,** 197–207, doi:10.1175/1520-0493(1992)120<0197:TEEOMW>2.0.CO;2.

Li, X., and Coauthors, 2009: Watershed Allied Telemetry Experimental Research. *J. Geophys. Res.,* **114,** D22103, doi:10.1029/2008JD011590.

——, and Coauthors, 2013: Heihe Watershed Allied Telemetry Experimental Research (HiWATER): Scientific objectives and experimental design. *Bull. Amer. Meteor. Soc.,* **94,** 1145–1160, doi:10.1175/BAMS-D-12-00154.1.

Lin, J. Y., C. T. Cheng, and K. W. Chau, 2006: Using support vector machines for long-term discharge prediction. *Hydrol. Sci. J.,* **51,** 599–612, doi:10.1623/hysj.51.4.599.

Liston, G. E., and K. A. Elder, 2006: Meteorological distribution system for high-resolution terrestrial modeling (MicroMet). *J. Hydrometeor.,* **7,** 217–234, doi:10.1175/JHM486.1.

Michalakes, J., J. Dudhia, D. B. Gill, J. B. Klemp, and W. Skamarock, 1998: Design of a next-generation regional weather research and forecast model. *Towards Teracomputing: Proceedings of the Eighth ECMWF Workshop on the Use of Parallel Processors in Meteorology,* W. Zwieflhofer and N. Kreitz, Eds., World Scientific, 117–124.

——, S. Chen, J. Dudhia, L. Hart, J. B. Klemp, J. Middlecoff, and W. Skamarock, 2001: Development of a next generation regional weather research and forecast model. *Developments in Teracomputing: Proceedings of the Ninth ECMWF Workshop on the Use of High Performance Computing in Meteorology,* W. Zwieflhofer and N. Kreitz, Eds., World Scientific, 269–276.

NCEP, 2014: NCEP FNL Operational Model Global Tropospheric Analyses, continuing from July 1999. Research Data Archive, NCAR Computational and Information Systems Laboratory, Boulder, CO, digital media, doi:10.5065/D6M043C6.

New, M., M. Hulme, and P. Jones, 1999: Representing twentieth-century space–time climate variability. Part I: Development of a 1961–90 mean monthly terrestrial climatology. *J. Climate,* **12,** 829–856, doi:10.1175/1520-0442(1999)012<0829:RTCSTC>2.0.CO;2.

——, ——, and ——, 2000: Representing twentieth-century space–time climate variability. Part II: Development of 1901–96 monthly grids of terrestrial surface climate. *J. Climate,* **13,** 2217–2238, doi:10.1175/1520-0442(2000)013<2217:RTCSTC>2.0.CO;2.

Pachauri, R. K., and A. Reisinger, Eds., 2007: *Climate Change 2007: Synthesis Report*. Intergovernmental Panel on Climate Change, 104 pp.

Prigent, C., 2010: Precipitation retrieval from space: An overview. *C. R. Geosci.,* **342,** 380–389, doi:10.1016/j.crte.2010.01.004.

Rodell, M., and Coauthors, 2004: The global land data assimilation system. *Bull. Amer. Meteor. Soc.,* **85,** 381–394, doi:10.1175/BAMS-85-3-381.

Sevruk, B., M. Ondras, and B. Chvila, 2009: The WMO precipitation measurement intercomparisons. *Atmos. Res.,* **92,** 376–380, doi:10.1016/j.atmosres.2009.01.016.

Skamarock, W. C., and Coauthors, 2008: A description of the Advanced Research WRF version 3. NCAR Tech. Note NCAR/TN-475+STR, 113 pp., doi:10.5065/D68S4MVH.

Smith, E. A., and Coauthors, 2007: International Global Precipitation Measurement (GPM) Program and Mission: An overview. *Measuring Precipitation from Space,* V. Levizzani, P. Bauer, and F. J. Turk, Eds., Advances in Global Change Research, Vol. 28, 611–653, doi:10.1007/978-1-4020-5835-6_48.

Song, K., E. Kang, Y. Lan, X. Zhang, Z. Zhang, B. Jin, and J. Zhang, 2003: Synchronous measurement of land surface processes in typical vegetation landscape zones in the Heihe River basin. *J. Glaciol. Geocryology,* **25,** 552–557.

Sorooshian, S., and Coauthors, 2011: Advancing the remote sensing of precipitation. *Bull. Amer. Meteor. Soc.,* **92,** 1271–1272, doi:10.1175/BAMS-D-11-00116.1.

Su, F., Y. Hong, and D. P. Lettenmaier, 2008: Evaluation of TRMM Multisatellite Precipitation Analysis (TMPA) and its utility in hydrologic prediction in the La Plata basin. *J. Hydrometeor.,* **9,** 622–640, doi:10.1175/2007JHM944.1.

Thornton, P. E., S. W. Running, and M. A. White, 1997: Generating surfaces of daily meteorological variables over large regions of complex terrain. *J. Hydrol.,* **190,** 214–251, doi:10.1016/S0022-1694(96)03128-9.

Tian, Y., C. D. Peter-Lidard, B. J. Choudhury, and M. Garcia, 2007: Multitemporal analysis of TRMM-based satellite precipitation products for land data assimilation applications. *J. Hydrometeor.,* **8,** 1165–1183, doi:10.1175/2007JHM859.1.

Tobin, C., A. Rinaldo, B. Schaefli, 2012: Snowfall limit forecasts and hydrological modeling. *J. Hydrometeor.,* **13,** 1507–1519, doi:10.1175/JHM-D-11-0147.1.

Wang, N. L., J. Q. He, X. Jiang, G. J. Song, J. C. Pu, X. B. Wu, and L. Chen, 2009: Study on the zone of maximum precipitation in the north slopes of the central Qilian Mountains. *J. Glaciol. Geocryology,* **31,** 395–403.

Ward, E., W. Buytaert, L. Peaver, and H. Wheater, 2011: Evaluation of precipitation products over complex mountainous terrain: A water resource perspective. *Adv. Water Resour.,* **34,** 1222–1231, doi:10.1016/j.advwatres.2011.05.007.

Wilby, R. L., and T. M. L. Wigley, 2000: Precipitation predictors for downscaling: Observed and general circulation model relationships. *Int. J. Climatol.,* **20,** 641–661, doi:10.1002/(SICI)1097-0088(200005)20:6<641::AID-JOC501>3.0.CO;2-1.

Wilk, J., D. Kniveton, L. Andersson, R. Layberry, M. C. Todd, D. Hughes, S. Ringrose, and C. Vanderpost, 2006: Estimating rainfall and water balance over the Okavango River basin for hydrological applications. *J. Hydrol.,* **331,** 18–29, doi:10.1016/j.jhydrol.2006.04.049.

Wilks, D., 1995: *Statistical Methods in the Atmospheric Sciences: An Introduction.* Academic Press, 467 pp.

Xie, P., and P. A. Arkin, 1996: Gauge-based monthly analysis of global land precipitation from 1971 to 1994. *J. Geophys. Res.,* **101,** 19 023–19 034, doi:10.1029/96JD01553.

——, and ——, 1997: Global precipitation: A 17-year monthly analysis based on gauge observations, satellite estimates, and numerical model outputs. *Bull. Amer. Meteor. Soc.,* **78,** 2539–2558, doi:10.1175/1520-0477(1997)078<2539:GPAYMA>2.0.CO;2.

Yin, Z. L., H. L. Xiao, S. B. Zou, Z. X. Lu, and W. H. Wang, 2013: Progress of the research on hydrological simulation in the mainstream of the Heihe River, Qilian Mountain. *J. Glaciol. Geocryology,* **35,** 438–446.

Zong, P., and H. Wang, 2011: Evaluation and analysis of RegCM3 simulated summer rainfall over the Huaihe River basin of China. *Acta Meteor. Sin.,* **25,** 386–394, doi:10.1007/s13351-011-0313-3.